JACS
JOURNAL OF THE AMERICAN CHEMICAL SOCIETY
Article
pubs.acs.org/JACS

Selective Catalytic Oxidative-Dehydrogenation of Carboxylic Acids—Acrylate and Crotonate Formation at the Au/TiO_2 Interface

Monica McEntee,[†] Wenjie Tang,[‡] Matthew Neurock,[†,‡] and John T. Yates, Jr*,[†,‡]

[†]Department of Chemistry, University of Virginia, Charlottesville, Virginia 22904, United States
[‡]Department of Chemical Engineering, University of Virginia, Charlottesville, Virginia 22904, United States

Supporting Information

ABSTRACT: The oxidative-dehydrogenation of carboxylic acids to selectively produce unsaturated acids at the second and third carbons regardless of alkyl chain length was found to occur on a Au/TiO_2 catalyst. Using transmission infrared spectroscopy (IR) and density functional theory (DFT), unsaturated acrylate ($H_2C{=}CHCOO$) and crotonate ($CH_3CH{=}CHCOO$) were observed to form from propionic acid (H_3CCH_2COOH) and butyric acid ($H_3CCH_2CH_2COOH$), respectively, on a catalyst with ∼3 nm diameter Au particles on TiO_2 at 400 K. Desorption experiments also show gas phase acrylic acid is produced. Isotopically labeled ^{13}C and ^{12}C propionic acid experiments along with DFT calculated frequency shifts confirm the formation of acrylate and crotonate. Experiments on pure TiO_2 confirmed that the unsaturated acids were not produced on the TiO_2 support alone, providing evidence that the sites for catalytic activity are at the dual Au−Ti^{4+} sites at the nanometer Au particles' perimeter. The DFT calculated energy barriers between 0.3 and 0.5 eV for the reaction pathway are consistent with the reaction occurring at 400 K on Au/TiO_2.

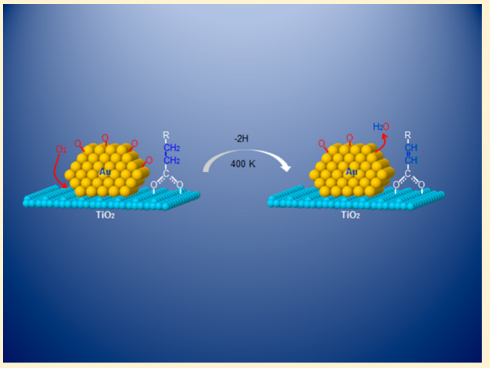

I. INTRODUCTION

The conversion of fatty acids derived from triglyceride-containing animal, vegetable, and algae oils into fuels and chemical intermediates requires catalytic deoxygenation, which is often carried out over supported Pd and other group VIII metal particles.[1−4] Long chain carboxylic acids can either undergo direct decarboxylation, which results in the formation of alkanes and CO_2, or a decarbonylation that produces olefins, CO, and water. The mechanisms for these reactions are still greatly debated and highly speculative. The Pd and Pt catalysts that are currently used are too active and unable to selectively produce α-olefins or other chemical intermediates in high yields.[1−3] In the present work, we use in situ IR spectroscopy, kinetics, and theory to show that Au nanoparticles supported on TiO_2 are highly selective in activating the C−H bonds at the C_2 and C_3 positions for linear organic acids (propionic and butyric acid) to form unsaturated carboxylate surface intermediates. The unique selectivity of Au/TiO_2 suggests that the sites and mechanism for the activation of organic acids are different from those active on supported Pd or Pt. These differences may provide clues for the design of catalytic engineering materials that are both highly active and selective.

Since Haruta's pioneering discovery[5] of the high oxidative catalytic activity for Au nanoparticles at low temperature and recent exciting high resolution electron microscopy studies,[6] well-defined kinetic in situ spectroscopic studies[7−9] and theoretical studies[10−12] have shown that the perimeter sites of Au nanoparticles supported on TiO_2 are responsible for the low temperature catalytic activity for the oxidation of H_2,[13,14] CO,[15−18] C_2H_4,[19] and acetic acid,[20,21] with reaction temperatures in the range 110−400 K. We have shown previously that the low temperature selective oxidation of C_2H_4 and acetic acid can be readily carried out over Au/TiO_2 catalysts, generating in both cases a ketenylidene intermediate on Au, $Au_2{=}C{=}C{=}O$.[19−21] In this paper, we report the observation of selective C=C double bond formation in higher carboxylic acids under oxidative-dehydrogenation conditions. The observed trend on Au/TiO_2 catalysts to selectively activate the C−H bonds at the C_2 and C_3 positions with respect to the COOH group in the organic acids, independent of alkyl chain length, is the result of the unique bifunctional characteristics of Au−Ti^{4+} perimeter sites for the oxidative-dehydrogenation of carboxylic acids.

Fourier transform transmission infrared spectroscopy (FTIR) and quadrupole mass spectrometry (QMS) were used together with density functional theory (DFT) calculations to help identify the oxidation products of two carboxylic acids and to discern the most likely reaction path to form unsaturated carboxylic acids on Au/TiO_2. This is the first account of the production of acrylate from propionic acid and crotonate from butyric acid on a Au/TiO_2 catalyst. We also show that facile reduction of the C=C bond in unsaturated carboxylic acids can be achieved using H_2 or D_2 on the Au/TiO_2 catalyst containing the unsaturated carboxylate species.

Received: January 27, 2014
Published: March 5, 2014

dx.doi.org/10.1021/ja500928h | J. Am. Chem. Soc. 2014, 136, 5116−5120

II. EXPERIMENTAL AND THEORETICAL PROCEDURES

The experiments were performed in a bakeable stainless steel high vacuum transmission IR chamber with a base pressure of ~1×10^{-8} Torr, pumped by both an ion pump and a turbo pump. A detailed description of the IR chamber is provided elsewhere.[13,15,22] The Au/TiO_2 catalyst was synthesized using a deposition-precipitation procedure provided by Zanella et al.[23] yielding Au particles with an average diameter of ~3 nm.[15] The weight percentage of Au was 8%. The TiO_2 powder is commercial Degussa P25 with a BET surface area of ~50 $m^2\ g^{-1}$. Acrylic acid (99.5%, extra pure, stabilized) was acquired from Fisher Scientific. Propionic acid (≥99.5%, ACS reagent), propionic-2,3-$^{13}C_2$ acid (99 atom % ^{13}C), and butyric acid (≥99.5%, analytical standard) were acquired from Sigma-Aldrich and further purified using the freeze−pump−thaw method. Oxygen gas (99.998%, Research Purity), D_2 gas, and H_2 gas (99.9995%, Research Purity) were acquired from Matheson Tri-Gas, Inc. Gas and liquid purity analysis along with desorption experiments were performed using a quadrupole mass (QMS) analyzer attached to the IR cell. Additionally, a GC−MS spectrometer was employed to analyze the liquid carboxylic acids.

The catalyst was heated in vacuum to 473 K and held at that temperature for 20 min before every experiment to help clean the surface and to prepare the catalyst for reaction. Oxygen at a pressure of ~18 Torr was then introduced to the catalyst at 473 K for ~3.5 h in order to remove traces of accumulated impurity hydrocarbon species. The cell was evacuated for 10 min, and ~2 Torr of H_2 was then introduced to the catalyst at 473 K for 10 min followed by evacuation for an additional 10 min. Finally, the catalyst was cooled to the desired reaction temperature of 400 K. Approximately 0.4 Torr of the desired carboxylic acid vapor was introduced into the cell followed by evacuation for 30 min at 400 K, forming a saturated layer of carboxylate species adsorbed on the TiO_2 support. One Torr of O_2 was then introduced into the cell, and over the course of 2.5 h, an FTIR spectrum was taken every minute during oxidation at the controlled sample temperature. Each FTIR spectrum takes 52 s and contains an average of 128 scans with a resolution of 2 cm^{-1}.

After oxidation of the desired acid followed by evacuation, 1 Torr of H_2 or D_2 was introduced into the cell at 400 K to carry out subsequent hydrogenation experiments, which were performed using IR spectroscopy or mass spectrometry. These experiments were performed immediately after catalytic oxidation of the carboxylic acid.

Density functional theory (DFT) calculations were carried out to examine the mechanism of acrylate formation and to determine the frequencies for adsorbed acrylate and crotonate species that form in order to compare with the experimental spectroscopic results. The TiO_2 support was simulated by using a (2 × 3) unit cell of the rutile TiO_2 (110) structure, with four O−Ti−O trilayers stacked in the Z-direction. The 3 nm Au particles supported on TiO_2 were simulated by a closely packed Au nanorod model anchored to the model TiO_2 (110) support. The Au nanorod provides Au sites with different coordination numbers (CN) ranging from 5 to 9 and has been used previously to successfully model catalytic reactions at the Au/TiO_2 interface.[10,15,16,20,24] More details of the model structure and calculation can be found in the Supporting Information.

III. RESULTS AND DISCUSSIONS

A. Frequency Identification Using FTIR and DFT.

During oxidation, an IR spectrum was taken every 60 s for 7810 s at 400 K. In order to capture the changes in the region below 1800 cm^{-1}, the oxidized propionate and butyrate spectra after 3070 s were measured by subtraction from their respective initial spectra before oxidation, as shown in Figure 1a.

Two characteristic absorbance bands formed at 1637 cm^{-1} and 1657 cm^{-1} during propionate and butyrate oxidation, respectively, on Au/TiO_2. These two bands are assigned to a >C═C< moiety at the C_2 and C_3 positions in both the bound propionate and butyrate species that form, respectively, converting them into acrylate and crotonate species. Others

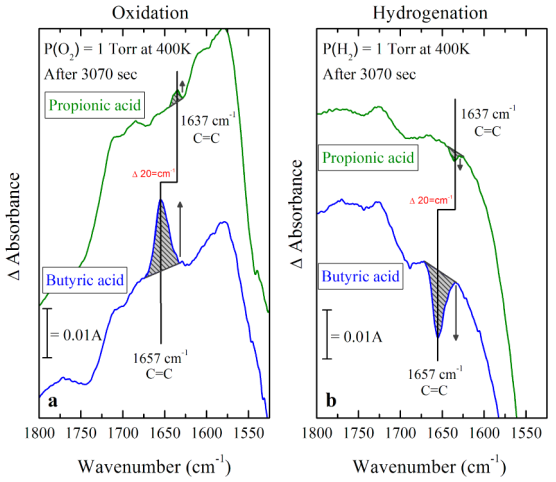

Figure 1. Developed spectra showing highlighted features in the C═C region of both propionic acid (green curve) and butyric acid (blue curve) after 3070 s of (a) oxidation and (b) subsequent hydrogenation on Au/TiO_2 at 400 K. The baseline in the selected (cross-hatched) features is drawn to guide the eye. The spectral features shown occur above an initial background, which has been subtracted. The spectral families associated with panel a are shown in Supporting Information Figures S1 and S2.

have assigned the C═C band for chemisorbed acrylate (CH_2═CHCOO*) and chemisorbed crotonate (CH_3CH═CHCOO*) on TiO_2[25,26] and other metal oxides[27,28] to similar frequencies near 1637 and 1659 cm^{-1}, respectively. Other possible oxidation products were investigated and ruled out according to their C═O and C═C mode frequencies on TiO_2 (See Table S1 in Supporting Information).

In order to determine if the formation of the two unsaturated carboxylate species required the presence of Au, the oxidation experiments were repeated on a blank TiO_2 catalyst at 400 K. No acrylate or crotonate were formed on TiO_2 alone, as shown in the Supporting Information Figures S1a and S2a. The oxidative-dehydrogenation activity, thus, appears to require Au sites. Previous results for the oxidation of CO, H_2, acetic acid, and ethylene showed that the activation and dissociation of O_2 occurs at the dual Au−Ti^{4+} site on the perimeter of Au nanoparticles and results in the formation of O adatoms bound to Au sites, which are rather basic and can participate in the activation of the C−H bonds of carboxylate intermediates bound to interfacial Ti^{4+} sites. Other groups[29] have also observed C−H bond activation due to oxygen at the Au/TiO_2 interface.

After the formation of these unsaturated carboxylate species, the cell was evacuated and one Torr of H_2 was introduced into the cell at 400 K for the same amount of time. Figure 1b shows the subtracted spectra for both the preoxidized propionate and butyrate on Au/TiO_2 after 3070 s in H_2. It can be seen that the same C═C absorption bands produced by the oxidative activation of the acid decrease in absorbance via reduction under H_2. The loss of these two bands is attributed to the hydrogenation of the unsaturated >C═C< bond, showing the reversibility of the oxidative-dehydrogenation and hydrogenation processes. To further verify that the 1637 cm^{-1} band is from >C═C< containing species (acrylate), 0.4 Torr of acrylic acid (CH_2═CHCOOH) was introduced onto the clean Au/TiO_2 surface at 400 K. Figure 2a shows bands at 1637, 1520, 1448, 1373, and 1271 cm^{-1}, which are attributed to acrylate species assigned to ν(C═C), $\nu_{as}(CO_2)$, $\nu_s(CO_2)$,

dx.doi.org/10.1021/ja500928h | J. Am. Chem. Soc. 2014, 136, 5116−5120

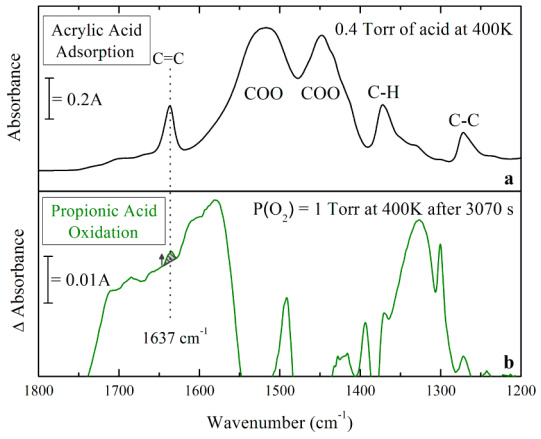

Figure 2. Comparison of (a) acrylic acid (black curve) and (b) propionic acid oxidation products (green curve from Figure 1a) on Au/TiO_2 at 400 K. The spectral features shown in (b) occur above an initial background.

δ(C−H), and ν(C−C), respectively.[25] The band at 1637 cm^{-1} assigned to the acrylate intermediate matches the ν(C═C) band formed during the oxidation of the surface propionate as shown in Figure 2b, establishing that oxidative-dehydrogenation of propionate is being observed specifically at the C_2 and C_3 positions of the acid. The loss of propionate during oxidation can be seen in Figure 2b with the negative bands around 1550−1500 cm^{-1} ($\nu_{as}(CO_2)$), 1460−1430 cm^{-1} ($\nu_s(CO_2)$), 1380 cm^{-1} ($\delta_s(CH_3)$), and 1300 cm^{-1} ($\delta(CH_2)$).[25] Unfortunately, the possible growth of other acrylate bands in these regions cannot be inferred.

Isotopically labeled propionic acid ($^{13}CH_3{}^{13}CH_2COOH$) oxidation experiments were also performed on Au/TiO_2 at 400 K. Figure 3a shows the difference spectra for both the propionate and ^{13}C-labeled propionate on Au/TiO_2 after 3070 s in O_2. The $^{13}C═{}^{13}C$ band is red-shifted by 45 cm^{-1} to 1592 cm^{-1}.

Our DFT calculation results indicate that the $^{12}C═{}^{12}C$ stretching frequencies for acrylate and $^{13}C_2$-acrylate appear at 1624 and 1576 cm^{-1}, respectively, as shown in Figure 4. The

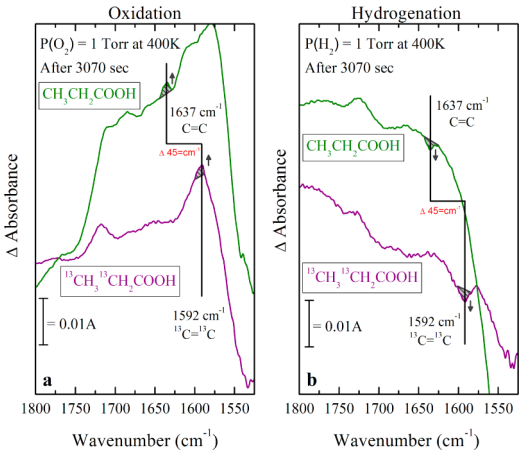

Figure 3. IR frequency shift comparison of the propionic acid (CH_3CH_2COOH) oxidation product (green curve) and the isotopically labeled propionic acid ($^{13}CH_3{}^{13}CH_2COOH$) oxidation product (purple curve) after 3070 s of (a) oxidation and subsequent (b) hydrogenation on Au/TiO_2 at 400 K.

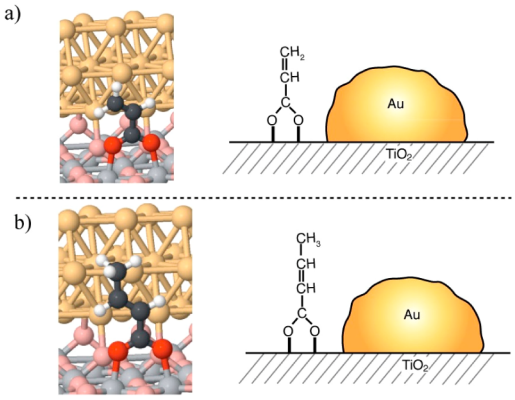

Molecule	DFT ν(C=C) cm^{-1}	DFT Isotopic Diff. cm^{-1}	Expl. ν(C=C) cm^{-1}	Expl. Isotopic Diff. cm^{-1}
CH_2=CHCOO	1624		1637	
$^{13}CH_2{=}{}^{13}CHCOO$	1576	48	1592	45
CH_3CH=CHCOO	1639		1657	

Figure 4. Structure of (a) acrylate and (b) crotonate bound to Ti^{4+} sites at the Au/TiO_2 perimeter. Their calculated C═C bond vibrational frequencies are listed in the table along with the experimental frequencies and shifts.

theoretical red shift between $^{12}C═{}^{12}C$ and $^{13}C═{}^{13}C$ frequencies is, therefore, 48 cm^{-1}, which is in very good agreement with the experimental difference of 45 cm^{-1} and well within the error of DFT. Subsequent hydrogenation experiments were performed as well, and both the $^{12}C═{}^{12}C$ and $^{13}C═{}^{13}C$ bands decrease in absorbance as shown in Figure 3b. These experiments and simulations provide convincing evidence that propionate dehydrogenates to acrylate under oxidation conditions.

Similarly, butyrate is found to convert into crotonate upon oxidative-dehydrogenation on Au/TiO_2. Figure 4 shows the DFT calculated C═C stretching frequency for crotonate, 1639 cm^{-1}, which is blue shifted by 15 cm^{-1} from the calculated acrylate C═C stretching frequency. This shift is consistent with the experimental shift of 20 cm^{-1} in comparing propionate and butyrate oxidation in Figure 1. It is likely that the second step in the oxidation mechanism after O_2 dissociation involves the oxidative activation of the C−H bond of the carboxylate at the C_2 site followed by the subsequent activation of the C−H bond at the C_3 site. These results are consistent with previous work by Green et al.,[21] where two H atoms were observed to be removed from the terminal methyl group on an acetate intermediate on TiO_2 by O atoms bound to neighboring Au sites in the initial steps in the oxidation of acetic acid at the Au/TiO_2 interface. This leads finally to the formation of the ketenylidene species, $Au_2C═C═O$, from acetic acid. The C−H bonds that sit α to carbonyl groups are weakly acidic and can be activated by basic oxygen intermediates that form on Au.[30,31]

B. Studies of Gas Phase Products Using QMS. After propionic acid oxidation the vacuum cell was evacuated, and the catalyst was cooled down to 375 K for 30 min. Then, the catalyst was systematically heated up to 600 K at 0.5 K/s with the cell open to the QMS for analysis of gas products coming off the surface. To avoid over pressurizing the QMS, the

dx.doi.org/10.1021/ja500928h | J. Am. Chem. Soc. 2014, 136, 5116−5120

catalyst was not heated higher than 600 K. As shown in Figure 5a, masses 72 and 71 start to desorb around 425 K and are

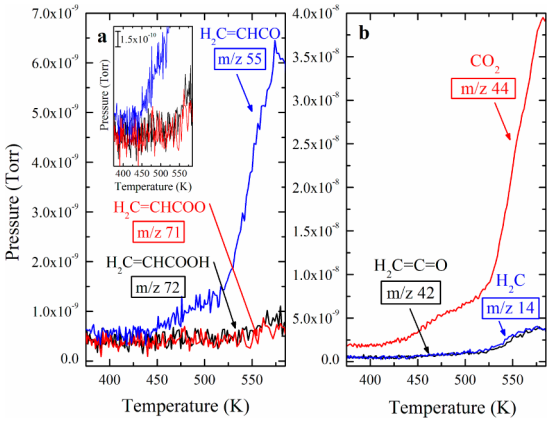

Figure 5. QMS desorption analysis of masses (a) 55 (H_2C═CHCO, blue), 71 (H_2C═CHCOO, red), and 72 (H_2C═CHCOOH, black) and (b) 14 (H_2C, blue), 42 (H_2C═C═O, black), and 44 (CO_2, red) after propionic oxidation on Au/TiO_2.

assigned to acrylic acid (black and red curves). The inset in Figure 5a is an enlarged view of these two masses. The cracking pattern for propionic acid does not contain these masses as shown in the Supporting Information Figure S3; therefore, the most likely molecule is acrylic acid, which is consistent with the IR and DFT frequency identifications on the surface discussed above.

Other desorption products were also observed with masses at 14, 42, 44, and 55. Mass 55 (H_2C═CHCO) is attributed to a mixture of mass spectrometer cracking products of both acrylic acid and propionic acid.

Further oxidation occurs to form a ketene species (H_2C═C═O) and a CH_2^+ cracking product as shown in Figure 5b by masses 14 and 42. Lastly, the major product to be formed from the oxidation of propionic acid is CO_2 at mass 44. Therefore, the acrylic acid and ketene species are side products or intermediates that eventually form the fully oxidized product, carbon dioxide.

Another desorption experiment was performed after the addition of D_2 at 400 K to the catalyst, which had previously caused propionic acid oxidation. This experiment was designed to follow up on the hydrogenation experiment in Figure 3. After an hour in D_2, the cell was evacuated and the catalyst was cooled to 375 K. Similar to the desorption method mentioned above, the catalyst was heated up to 600 K and the QMS was used for gas analysis. Figure 6 shows masses at 75 ($CH_2DCHDCOO$) and 76 ($CH_2DCHDCOOH$), which are attributed to deuterated propionic acid (black and red curves) with 2 D atoms. Similarly, mass 59 is attributed to a mixture of propionic acid with the OH group replaced with a D atom (CH_3CH_2COD) and propionic acid without the OH group and containing 2 D atoms ($CH_2DCHDCO$). These mass assignments are consistent with the deuteration of the unsaturated molecules that were produced in the oxidation experiments. Therefore, in agreement with the disappearance of the C═C bands during hydrogenation, the appearance of these deuterated molecules is attributed to the deuteration of the unsaturated species produced in Figure 5a.

C. DFT Energy Pathway to Form Acrylate on Au/TiO_2. The mechanism for the formation of acrylate from propionic

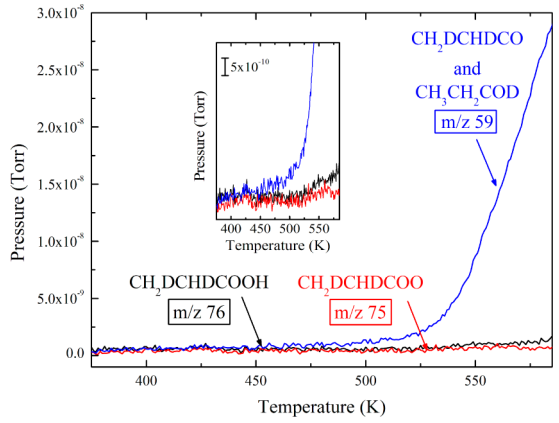

Figure 6. QMS desorption analysis of masses 59 ($CH_2DCHDCO$, blue), 75 ($CH_2DCHDCOO$, red), and 76 ($CH_2DCHDCOOH$, black) after the subsequent addition of D_2 to propionate + Au/TiO_2.

acid was examined here by carrying out density functional theory calculations. The calculated potential energy diagram for this reaction is shown in Figure 7. The detailed atomic

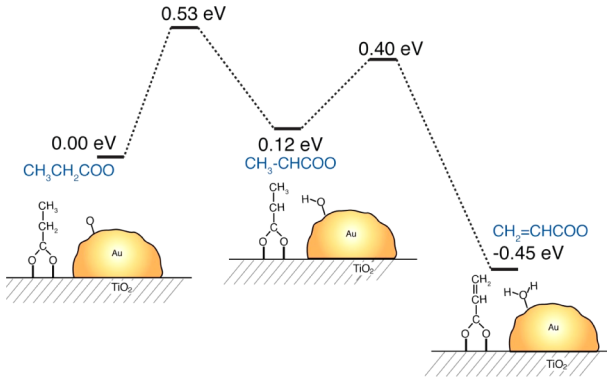

Figure 7. DFT-calculated potential energy diagram for the oxidative dehydrogenation of propionate at the Au/TiO_2 interface to form an acrylate surface intermediate.

structures for all of the reactants, intermediates, and products reported in Figure 7 are presented in Supporting Information Figure S4. Previously, we showed that O_2 is activated at Au–Ti^{4+} site pairs at the Au/TiO_2 interface with a barrier of ~0.5 eV and results in the formation of adsorbed atomic oxygen (O*) on the Au sites at the Au/TiO_2 perimeter.[15] The atomic oxygen that results is weakly bound to Au and acts as a base that can effectively activate the C–H bonds involved in the oxidative dehydrogenation.[21] The influence of basic O* on Au in activating O–H as well as C–H bonds has been discussed previously.[29−33] The O–H bond of propionic acid is readily cleaved by the bridging oxygen sites on the TiO_2 surface, resulting in the formation of surface propionate intermediates at the Au/TiO_2 interface. A C–H bond at the C_2 position can then be activated by the basic O* species bound to nearby Au sites. The C_2–H bond is activated before the C_3–H bond, as it is weaker and more acidic than the C_3–H bond. Also, steric hindrance at the bulky CH_3 group decreases its reactivity according to DFT calculations. This steric repulsion effect may be partially compensated by a stabilization due to charge delocalization over the alkyl chain. The barrier to activate the C_2–H bond via the O* bound to Au was calculated to be 0.53 eV, resulting in the formation of the CH_3CH–COO* species

dx.doi.org/10.1021/ja500928h | J. Am. Chem. Soc. 2014, 136, 5116−5120

that is bound to Ti sites on the oxide and an OH* intermediate bound to a neighboring Au site. This OH* species is even more basic than O* and can subsequently activate the C_3−H bond of the CH_3CHCOO/Ti species with a barrier of only 0.28 eV, thus resulting in the formation of TiO_2-bound acrylate (CH_2═CH−COO/Ti) and H_2O bound to Au. The acrylate is 0.45 eV more stable than the original CH_3CH_2COO/Ti because of the formation of the C═C bond. All of the steps in this cycle involve activation barriers that range from 0.3 to 0.5 eV, thus indicating that the reaction can be carried out at moderate temperatures near 400 K as observed experimentally. Acrylate formation may occur at even lower temperatures; however, we chose 400 K as the ideal reaction temperature to observe all of the oxidation products for carboxylic acid oxidation on Au/TiO_2.

IV. CONCLUSION

The oxidative-dehydrogenation of carboxylate intermediates formed via the dissociative adsorption of two organic acids over a Au/TiO_2 catalyst has been studied by transmission IR methods and density functional theory calculations. For both the C_2 and C_3 acids, the C−H activation of the alkyl backbone occurs first at the C_2 atom, followed by the subsequent C−H activation at the C_3 atom to form a C═C moiety. The dual Au−Ti^{4+} sites that exist at the perimeter of nominally 3 nm Au particles supported on TiO_2 appear to be the active sites as they can readily activate both O_2 (as well as the organic acid) to form Au−O surface species that can subsequently activate the C−H bonds. The activity and selectivity observed is consistent with other partial oxidation processes observed on these special sites.[19−21] DFT calculations of the energy pathway are consistent with the temperature required for the reaction and also provide theoretical confirmation of vibrational assignments, comparing ^{12}C- and ^{13}C-labeled species. Both acrylate and crotonate, unsaturated carboxylate species, and their corresponding acids are observed on the surface by IR spectroscopy and in the gas phase by mass spectrometry. Additionally, the Au/TiO_2 catalyst also catalyzes the hydrogenation of the unsaturated carboxylate species.

■ ASSOCIATED CONTENT

Ⓢ Supporting Information

Control experiments along with detailed calculation parameters. This material is available free of charge via the Internet at http://pubs.acs.org.

■ AUTHOR INFORMATION

Corresponding Author

J. T. Yates, Jr. E-mail: johnt@virginia.edu.

Notes

The authors declare no competing financial interest.

■ ACKNOWLEDGMENTS

We gratefully acknowledge the financial support of this work from the Department of Energy—Office of Basic Energy Sciences under grant number DE-SC0002365 and the fellowship for Monica McEntee from AES Corporation through the AES Graduate Fellowships in Energy Research Program at the University of Virginia. We thank the Texas Advanced Computing Center for computing resources. We also thank the FIRST Center, an Energy Frontier Research Center funded by the U.S. Department of Energy, Office of Science, Office of Basic Energy Sciences for the partial support of Wenjie Tang.

■ REFERENCES

(1) Bernas, H.; Eränen, K.; Simakova, I.; Leino, A.; Kordás, K.; Myllyoja, J.; Mäki-Arvela, P.; Salmi, T.; Murzin, D. Y. *Fuel* **2010**, *89*, 2033−2039.

(2) Immer, J. G.; Kelly, M. J.; Lamb, H. H. *Appl. Catal., A* **2010**, *375*, 134−139.

(3) Simakova, I.; Rozmysłowicz, B.; Simakova, O.; Mäki-Arvela, P.; Simakov, A.; Murzin, D. Y. *Top. Catal.* **2011**, *54*, 460−466.

(4) Peng, B.; Zhao, C.; Kasakov, S.; Foraita, S.; Lercher, J. A. *Chem.—Eur. J.* **2013**, *19*, 4732−4741.

(5) Haruta, M.; Tsubota, S.; Kobayashi, T.; Kageyama, H.; Genet, M. J.; Delmon, B. *J. Catal.* **1993**, *144*, 175−192.

(6) Akita, T.; Kohyama, M.; Haruta, M. *Acc. Chem. Res.* **2013**, *46*, 1773−1782.

(7) Chen, M.; Goodman, D. *Science* **2004**, *306*, 252−255.

(8) Rodriguez, J.; Ma, S.; Liu, P.; Hrbek, J.; Evans, J.; Perez, M. *Science* **2007**, *318*, 1757−1760.

(9) Kotobuki, M.; Leppelt, R.; Hansgen, D.; Widmann, D.; Behm, R. *J. Catal.* **2009**, *264*, 67−76.

(10) Laursen, S.; Linic, S. *Phys. Chem. Chem. Phys.* **2009**, *11*, 11006−11012.

(11) Wang, J.; Hammer, B. *Phys. Rev. Lett.* **2006**, *97*, 136107.

(12) Hammer, B.; Norskov, J. *Nature* **1995**, *376*, 238−240.

(13) Green, I. X.; Tang, W.; Neurock, M.; Yates, J. T., Jr. *Angew. Chem., Int. Ed.* **2011**, *50*, 10186−10189.

(14) Fujitani, T.; Nakamura, I.; Akita, T.; Okumura, M.; Haruta, M. *Angew. Chem.* **2009**, *121*, 9679−9682.

(15) Green, I. X.; Tang, W.; Neurock, M.; Yates, J. T., Jr. *Science* **2011**, *333*, 736−739.

(16) Green, I. X.; Tang, W.; McEntee, M.; Neurock, M.; Yates, J. T., Jr. *J. Am. Chem. Soc.* **2012**, *134*, 12717−12723.

(17) Kung, M. C.; Davis, R. J.; Kung, H. H. *J. Phys. Chem. C* **2007**, *111*, 11767−11775.

(18) Kung, H.; Kung, M.; Costello, C. *J. Catal.* **2003**, *216*, 425−432.

(19) Green, I. X.; McEntee, M.; Tang, W.; Neurock, M.; Yates, J. T., Jr. *Top. Catal.* **2013**, *56*, 1512−1524.

(20) Green, I. X.; Tang, W.; Neurock, M.; Yates, J. T., Jr. *J. Am. Chem. Soc.* **2012**, *134*, 13569−13572.

(21) Green, I. X.; Tang, W.; Neurock, M.; Yates, J. T., Jr. *Faraday Discuss.* **2013**, *162*, 247−265.

(22) Basu, P.; Ballinger, T.; Yates, J. T., Jr. *Rev. Sci. Instrum.* **1988**, *59*, 1321−1327.

(23) Zanella, R.; Giorgio, S.; Henry, C. R.; Louis, C. *J. Phys. Chem. B* **2002**, *106*, 7634−7642.

(24) Molina, L.; Rasmussen, M.; Hammer, B. *J. Chem. Phys.* **2004**, *120*, 7673−7680.

(25) Chen, Y. K.; Lin, Y. F.; Peng, Z. W.; Lin, J. L. *J. Phys. Chem. C* **2010**, *114*, 17720−17727.

(26) Lochar, V.; Pytel, M.; Smolakova, L. *Sci. Pap. Univ. Pardubice, Ser. A* **2009**, *15*, 121−127.

(27) Coast, R.; Pikus, M.; Henriksen, P. N.; Nitowski, G. A. *J. Phys. Chem.* **1996**, *100*, 15011−15014.

(28) Harrison, P. G.; Maunders, B. *J. Chem. Soc., Faraday Trans. 1* **1985**, *81*, 1345−1355.

(29) Camellone, M. F.; Zhao, J.; Jin, L.; Wang, Y.; Muhler, M.; Marx, D. *Angew. Chem., Int. Ed.* **2013**, *52*, 5780−5784.

(30) Madix, R. J.; Roberts, J. T. *Surface Reactions*; Springer-Verlag: New York, 1994.

(31) Liu, X.; Madix, R. J.; Friend, C. M. *Chem. Soc. Rev.* **2008**, *37*, 2243−2261.

(32) Green, I. X.; Tang, W.; Neurock, M.; Yates, J. T., Jr. *Acc. Chem. Res.* **2013**, No. 10.1021/ar400196f.

(33) Zope, B. N.; Hibbitts, D. D.; Neurock, M.; Davis, R. J. *Science* **2010**, *330*, 74−78.